Repeated Large-Magnitude Earthquakes in the Marianna Area of East-Central Arkansas During the Middle-Early Holocene and Possibly the Late Pleistocene

Martitia P. Tuttle[*1], Haydar Al-Shukri[2], Hanan Mahdi[2], Rauf Hussein[3], Taher Ameen[2], Steven L. Forman[4], Kathleen Dyer-Williams[5], Kathleen Tucker[6], Martha Kopper[7], Muntadher Al-Kaabi[2], and Okba R. Al-Qadhi[8]

Abstract

Very large, weathered sand blows and related sand dikes in the Marianna area indicate that large earthquakes were centered there in the past. Radiocarbon (^{14}C) and optically stimulated luminescence dating suggest that the liquefaction features formed during paleoearthquakes about 4.7, 5.4, 6.8, and 9.8 thousand years ago (ka) and possibly during two earlier events about <19.5 and <24.3 ka. Many sand blows occur along or near a northwest-oriented tonal lineament—known as the Daytona Beach lineament (DBL)—located southwest of Marianna. Supported by an independent seismic reflection study that identified a fault zone beneath the lineament, the DBL and spatially associated sand blows may be the surface expression of an active fault zone. Sand blows along the lineament at sites DB1, DBSE2, DBNW2, DBNW3, and DBNW5 are elongated in a northwest–southeast direction and have sand dikes with northwest trends. At sites DBSE2 and DBNW2, soft-sediment faults, also with northwest trends, crosscut sand dikes, displacing soil lamellae within the dikes. At one of the sites, small sand dikes were injected along the faults. Northeast of Marianna at site SF500, a compound sand blow composed of multiple depositional units formed about 6.8 ka. Located near the intersection of the White River fault zone and Eastern Reelfoot Rift Margin fault zone, the compound sand blow likely formed as the result of a sequence of large earthquakes, perhaps produced by these fault zones. Liquefaction potential analysis suggests that moment magnitude (M) 6.0–6.5 earthquakes generated by the fault zone beneath the DBL could have induced liquefaction in the Marianna area. However, larger Marianna earthquakes ranging up to M 7.5 would be required to induce liquefaction at distal sites near Blytheville and Marked Tree, Arkansas, and Tunica, Mississippi, where relatively small liquefaction features may have formed during the 4.7, 5.4, and 6.8 ka events.

Cite this article as Tuttle, M. P., H. Al-Shukri, H. Mahdi, R. Hussein, T. Ameen, S. L. Forman, K. Dyer-Williams, K. Tucker, M. Kopper, M. Al-Kaabi, and O. R. Al-Qadhi (2026). Repeated Large-Magnitude Earthquakes in the Marianna Area of East-Central Arkansas During the Middle-Early Holocene and Possibly the Late Pleistocene, *Seismol. Res. Lett.* **97**, 715–729, doi: 10.1785/0220250324.

Supplemental Material

Introduction

Twenty years ago, large weathered sand blows and related sand dikes were discovered in the Marianna area, located about 70 km southwest of Memphis, Tennessee, and 80 km south of the New Madrid seismic zone (NMSZ) (Figs. 1 and 2; Al-Shukri *et al.*, 2005). The discovery came as a surprise since no large historical earthquakes had been reported in the Marianna area, and only a few small earthquakes had been recorded there during the instrumental period, which effectively began in 1974. The sand blows were identified on satellite images and verified in the field. They were excavated and found to be deeply weathered, suggesting that they were thousands of years old. ^{14}C dating indicated that sand blows at the Nancy1 and Nancy2 sites formed about 4.7 and 5.4 ka, respectively (Fig. 2, Fig. S1 in the supplemental material available to this article, Table 1). Given that they were as large as,

1. M. Tuttle & Associates, Georgetown, Maine, U.S.A.; 2. School of Physical Sciences, Physics Program, University of Arkansas at Little Rock, Little Rock, Arkansas, U.S.A., https://orcid.org/0000-0001-9090-1029 (HA-S); https://orcid.org/0000-0002-2747-1465 (HM); https://orcid.org/0000-0002-8083-1191 (TA); https://orcid.org/0009-0000-2594-5260 (MA-K); 3. Parks and Recreation Department, City of Cape Coral, Cape Coral, Florida, U.S.A., https://orcid.org/0000-0002-3441-7600 (RH); 4. Department of Geosciences, Baylor University, Waco, Texas, U.S.A., https://orcid.org/0000-0002-2080-7915 (SLF); 5. VanLeen and Associates, Columbia, Maryland, U.S.A.; 6. PangaeaGIS, Memphis, Tennessee, U.S.A.; 7. Office of the State Geologist of Arkansas, North Little Rock, Arkansas, U.S.A.; 8. Columbus State Community College, Grove City, Ohio, U.S.A.

*Corresponding author: mptuttle@earthlink.net

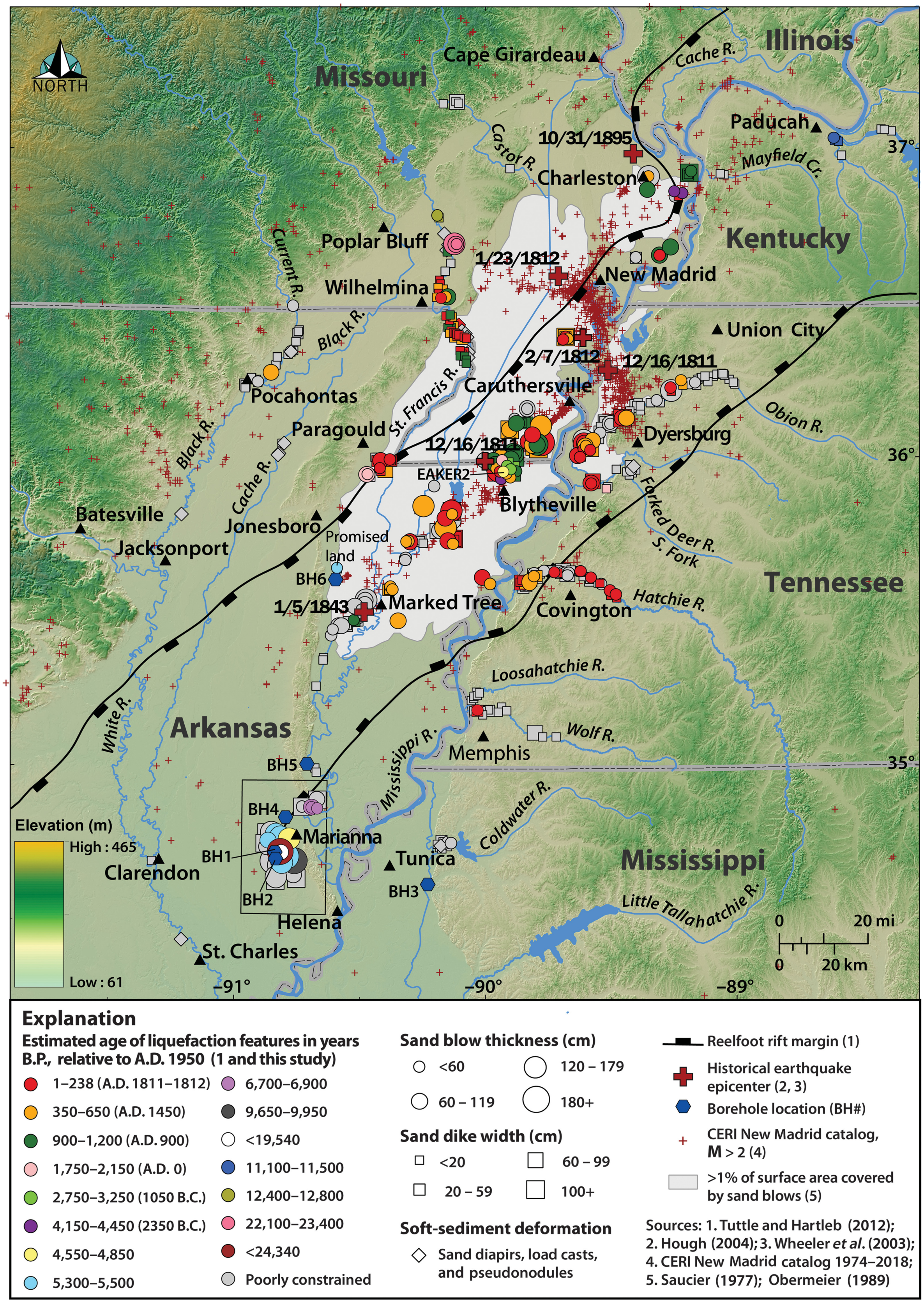

Figure 1. Shaded relief map of the Marianna area (outlined by a black rectangle) and the New Madrid seismic zone (NMSZ) (delineated by seismicity), showing locations, measured sizes, and estimated ages of earthquake-induced liquefaction features. The Marianna area is located near the southern end of the eastern Reelfoot Rift margin fault zone. Sources of information are listed in the Explanation.

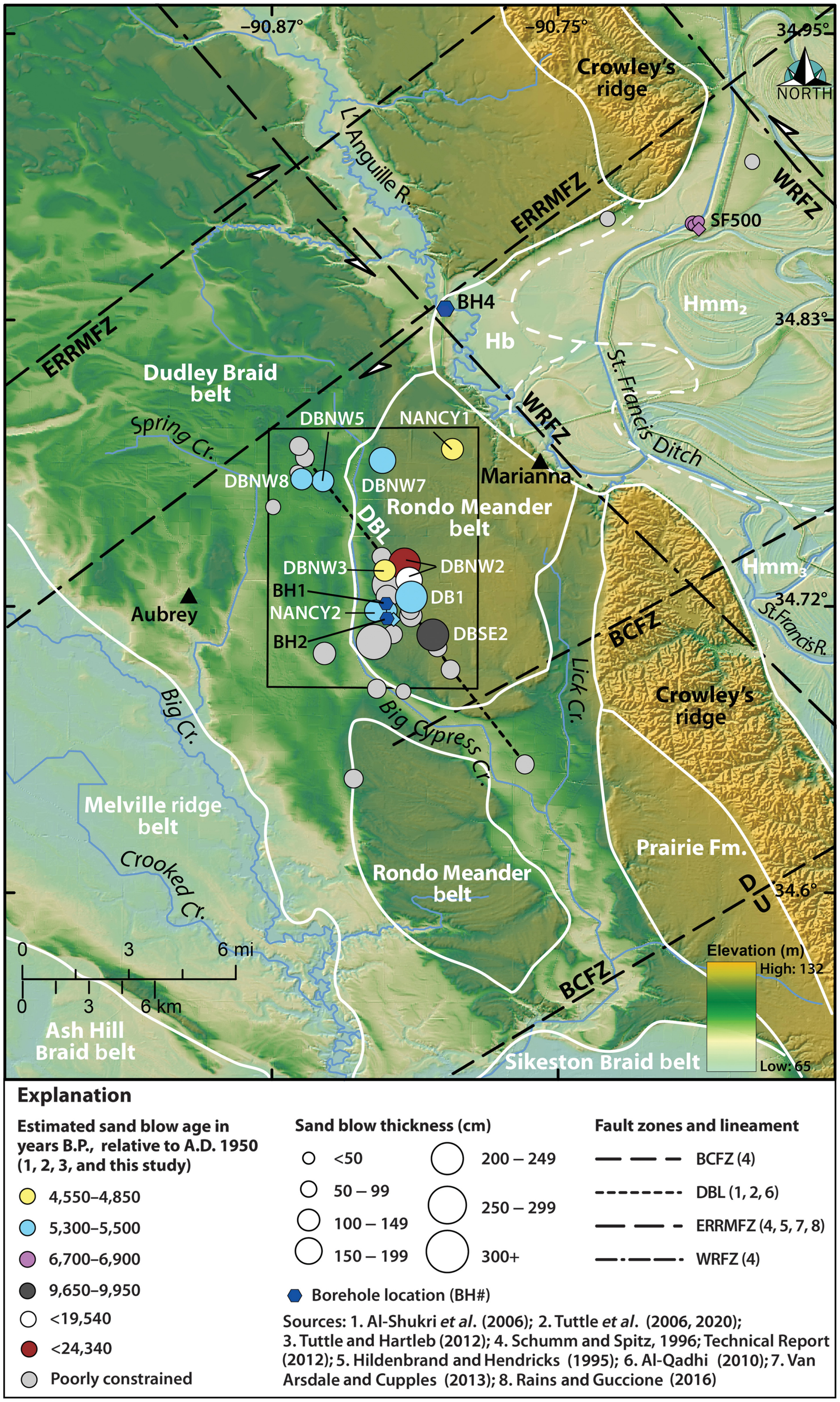

Figure 2. Shaded relief map of the Marianna area (delineated in Fig. 1 with a black rectangle), showing the DBL as well as locations, measured sizes, and estimated ages of sand blows investigated during this and previous studies. Morphostratigraphic units mapped by Rittenour *et al.* (2007) are outlined by white lines. Study sites along the DBL occur in the Pleistocene deposits of the Dudley Braid and Rondo Meander Belts, whereas SF500 occurs in Holocene deposits of the Mississippi River meander belt (Hmm). Borehole abbreviated as BH. Fault zones: BCFZ, Big Creek fault zone; DBL, Daytona Beach lineament; ERRMFZ, eastern Reelfoot rift margin fault zone; and WRFZ, White River fault zone. Sources of information are listed in the explanation.

yet older than, sand blows in the NMSZ, the Marianna sand blows likely formed as the result of large earthquakes centered in the Marianna area (Al-Shukri *et al.*, 2005). A subsequent investigation of a large sand blow at the Daytona Beach 1 (DB1) site corroborated an event about 5.4 ka (Table 1) (Tuttle *et al.*, 2006). The DB1 sand blow and other sand blows were found to occur along a northwest-oriented lineament, named the DBL, which is at least 12 km in length (Al-Qadhi, 2010; Fig. 2, Fig. S1). The DBL is relatively straight, subparallel to the nearby White River fault zone (WRFZ), and might be related to a family of northwest-oriented faults in the region.

To test the hypothesis that the DBL is related to faulting at depth, seismic-reflection data were collected along two transects that crossed the lineament in the vicinity of DB1, Nancy2, and DBSE2 (Odum *et al.*, 2016; see Fig. S1). The seismic-reflection profiles revealed a zone of near-vertical faults directly below the DBL in the 100–1100 m depth range, likely including Eocene through Paleozoic strata (Odum *et al.*, 2016). The seismic-reflection study also found that fault displacements increase with depth, suggesting long-term recurrent faulting. These findings support the interpretation that the DBL and the large sand blows along it are the surface expression of an active fault zone that has repeatedly produced large earthquakes during the Holocene (0–0.0117 million years ago, or Ma; Tuttle *et al.*, 2006, 2020; Al-Shukri *et al.*, 2009, 2015; Cohen *et al.*, 2022).

TABLE 1
Summary of Earthquake-Induced Liquefaction Features, Age Information, and Event Timing

Site Name	Sand Blow Thickness (cm)	Dike Width (cm)	Dike Strike/Dip	Weathering	Age Constraint Yr B.P. (1950)*	Event Timing (ka)
DB1†	245	122	N10°W/84° NE	Upper 75–150 cm iron-stained and bioturbated	≤5,440 ± 130	5.4
DBSE2	220	130	N20°W/80° NE, N23°W/78° NE	Iron-stained, redoximorphic features, Fe–Mn nodules, soil lamellae, and silt accumulation	≤9,795 ± 115	9.8
		~500	N35–50°W/73° NE			
		70	N23°W/50° NE			
DBNW2						
S trench	160	640	N43°W/86° NE	Similar but less iron-stained and fewer soil lamellae	≤19,540 ± 1,010	<19.5
N trench	240	450	N36°W/86° NE	Iron-stained, redoximorphic features, 1.5 m section of soil lamellae, silt accumulation	≤24,340 ± 1,790	<24.3
DBNW3						
N trench	75	17, 4	N55°W/86° NE, N41°W/87° NE	Iron-stained, few Fe–Mn nodules and soil lamellae	<4,689 ± 116	4.7
S trench	100	72–100	N39°W/71° NE	Similar	<4,710 ± 215	
DBNW5	140	270	N45°W/steep	Iron-stained, Fe–Mn nodules	≤5,402 ± 75	5.4
DBNW7	150	49	N5°E/79°–90° E	Iron-stained, redoximorphic features, Fe–Mn nodules	≤5,402 ± 75	5.4
DBNW8	105	50–54, 50 and 16	N36°E/37° SE, N21°E/42° SE, N48°E/66° SE	Iron-stained, redoximorphic features, few soil lamellae	≤5,402 ± 75	5.4
Nancy1‡	120	20 multiple	NW/90°	Iron-stained and redoximorphic features	<4,825 ± 25	4.7
Nancy2‡						
Trench 1	118	15	N25°E/10–15° NW	Iron-stained and redoximorphic features	<5,620 ± 40	5.4
Trench 2	130	20	N35°E/44° NW	Similar	≤5,460 ± 130	
SF500†	42, 5, 60, 18, 42	12, 5, 13, 8, 7, 6, 2, 16, 4, 4	Not measured; trending NW	Relatively unweathered due to burial by swamp deposits	≥6,805 ± 95, ~6,810 ± 400	6.8

N, north; NW, northwest; S, south.
*Calibrated ^{14}C ages and optically stimulated luminescence (OSL) ages in years B.P. or before A.D. 1950; < means after, ≤ means during or after, ≥ means during or before, ~ means approximately.
†From Tuttle *et al.* (2006).
‡From Al-Shukri *et al.* (2005).

About 18 km northeast of the DBL, a compound sand blow was found at site SF500 during reconnaissance along the St. Francis drainage ditch (Fig. 2; Tuttle *et al.*, 2006). The sand blow is composed of five depositional units and related sand dikes, similar to compound sand blows in the NMSZ that formed as a result of the 1811–1812 earthquake sequence. This suggests that the St. Francis features also formed as a result of a sequence of earthquakes. The lower four units are stratigraphically consistent with no intervening soil development or deposition, indicating that they formed over a short period of time, perhaps days to weeks. The uppermost unit is interbedded with the basal portion of the overlying backswamp sediment, indicating a dramatic change in environment from fluvial to backswamp deposition. Geochronology at the site suggests that the liquefaction features formed about 6.8 ka (Tuttle *et al.*, 2006). SF500 is located within the WRFZ and near its intersection with the ERRMFZ. These fault zones are possible sources of the sequence of earthquakes responsible for the formation of the compound sand blow and may have played a role in altering the environment of deposition in the area.

Based on the findings of our paleoliquefaction studies, the Marianna area was recognized as a significant earthquake source and included in the Central and Eastern U.S. Seismic Source Characterization project (CEUS SSCP; Technical Report, 2012) and the 2014 National Probabilistic Seismic Hazard Maps (Petersen *et al.*, 2014). The Marianna source was subsequently retained in the 2023 National Seismic Hazard Model (Thompson Jobe *et al.*, 2022). Paleoliquefaction studies have been ongoing in the Marianna area and include additional investigations of sand blows, dating of liquefaction features to further constrain event timing, and liquefaction potential analysis of scenario earthquakes to help interpret locations and magnitudes of past earthquakes. This article presents the results of these recent studies and updates the interpretation of the earthquake potential of the Marianna area. New information gained about the timing, magnitude, and recurrence of paleoearthquakes in the Marianna area and on the northwest-oriented fault zone beneath the DBL is likely to contribute to the regional assessment of earthquake hazards and the National Seismic Hazard Model. In addition, this article relays important lessons learned about dating old, weathered sand blows, which will contribute to future paleoliquefaction studies in the Marianna area and elsewhere.

Methodology

Site investigations

Numerous large sand blows occur in the Marianna area and appear on satellite images as elliptical, light-colored domains. Sites are identified that have the potential to broaden the spatial and temporal information about earthquake-induced liquefaction in the area. Study sites are visited and test pits excavated to confirm that the light-colored domains are composed of sandy soils, which differ from the surrounding dark-colored, silty soils developed in Late Pleistocene Peoria Loess deposits.

Most study sites in the Western Lowlands west of Marianna occur in the Rondo meander belt, except for study sites DBNW5 and DBNW 8, which are situated to the west in the Dudley braid belt (Fig. 2; Rittenour *et al.*, 2007). Both morphostratigraphic units are characterized by Peoria Loess, deposited about 12–25 ka (McKay, 1979; Ruhe, 1983), overlying fluvial deposits, including sand (Rittenour *et al.*, 2007). Rondo meander belt deposits have a thicker section of loess and finer fluvial section than Dudley braid belt deposits. The Dudley braid belt crosscuts the scroll-bar topography of the Rondo meander belt, suggesting it is younger. Optically stimulated luminescence (OSL) dating of samples collected within the Dudley and Rondo fluvial sections yielded ages of 46–69 ka and 76–90 ka, respectively (Rittenour *et al.*, 2007).

According to The Soil Survey of Lee County, Arkansas (Gray, 1977), the soils mapped on the Rondo and Dudley surfaces west of Marianna are predominantly loamy soils formed in thick loess deposits. The Loring–Memphis–Grenada and Calloway–Henry–Loring soil associations are mapped in the area of the study sites. All these soils are Alfisols, silty, and have profiles generally in the form of A/B/C or A/B horizons, indicating that they formed from one parent material. Also, Marvell and LaGrange soils have been mapped at or very close to the study sites. These soils are also Alfisols, but they are composed of fine sandy loam overlying silt loam and have profiles in the form of A/B/IIB horizons, indicating two different parent materials. We think it is likely that the sandy loam of Marvell and LaGrange soils formed in sand vented from below as a result of earthquake-induced liquefaction; whereas the silt loam below the sandy loam formed in loess deposits like other soils in the area.

If a site appears to be promising and is selected for further evaluation, a ground-penetrating radar (GPR) survey is conducted, usually with a 400 MHz antenna, to determine whether or not the sand deposit is underlain by a sand dike (Fig. 3; Al-Shukri *et al.*, 2006; Chlaib *et al.*, 2014). A sand dike, which marks the fissure through which water and entrained sand vented to the ground surface as a result of earthquake-induced liquefaction, must be present to interpret a sand deposit as a sand blow (Tuttle and Hartleb, 2012; Tuttle, Hartleb, *et al.*, 2019). GPR surveys are also used to determine the extent and dimensions of the sand blows and sand dikes, and to site trenches for further study of the liquefaction features and collection of samples for dating the features.

Trenches are sited so that they cross and expose both sand blows and related sand dikes. Trench walls are cleaned and logged at a scale of 1″ on log = 25 cm or 50 cm of trench wall, depending on the complexity of the liquefaction features (Fig. 4). Liquefaction features and their host sediment are described in terms of sedimentological and weathering characteristics. The size, orientation, vertical and horizontal displacements, and crosscutting relations of liquefaction features are documented. In addition, samples are collected to constrain the ages of the sand blows as narrowly as possible. Organic samples are collected for ^{14}C dating from soils buried by the sand blows and from remnants of soils below the modern plow zone, as well as tree root casts in the upper portions of the sand blows. Sediment samples for OSL dating are collected from sand blows, tops of buried soils, and subsoils.

Dating of sand blows and paleoearthquakes

Beta Analytic, Inc. dated organic samples using accelerator mass spectrometry (AMS). The AMS ages have errors of only ±30 yr and are calibrated using the probability density range method and the INTCAL20 database (Bronk Ramsey, 2009; Reimer *et al.*, 2020). Calibrated ^{14}C ages and calendar dates with error ranges of both 1 standard deviation (68.2% probability) and 2 standard deviations (95.4% probability) are provided in

Table S1. Results of ^{14}C dating are also presented in the site investigation summaries and on the trench logs, as well as in the supplement.

U.S. Geological Survey (USGS) OSL laboratory in Denver dated sediment samples collected at sites DBSE2 in 2010 and DBNW2 in 2015; whereas Geoluminescence Dating Laboratory at Baylor University dated samples collected later at sites DBNW3, DBNW5, DBNW7, and DBNW8. Systematic and random errors are calculated at one standard deviation (Forman *et al.*, 2000;

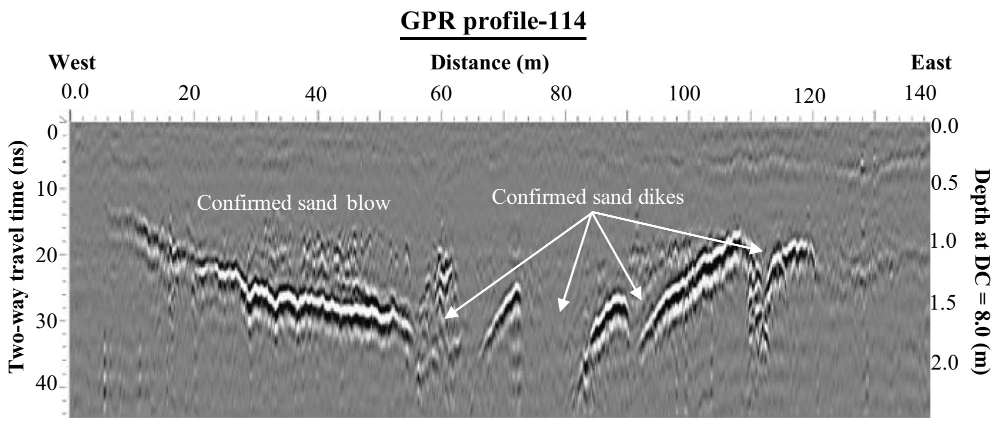

Figure 3. Example of a ground-penetrating radar (GPR) profile, GPR profile-114 from site DBSE2 (see Fig. S2 for location of profile), showing subsurface anomalies associated with a sand blow and related sand dikes (Al-Qadhi, 2010). The black and white bands represent the contact between the overlying sand blow and the underlying buried soil.

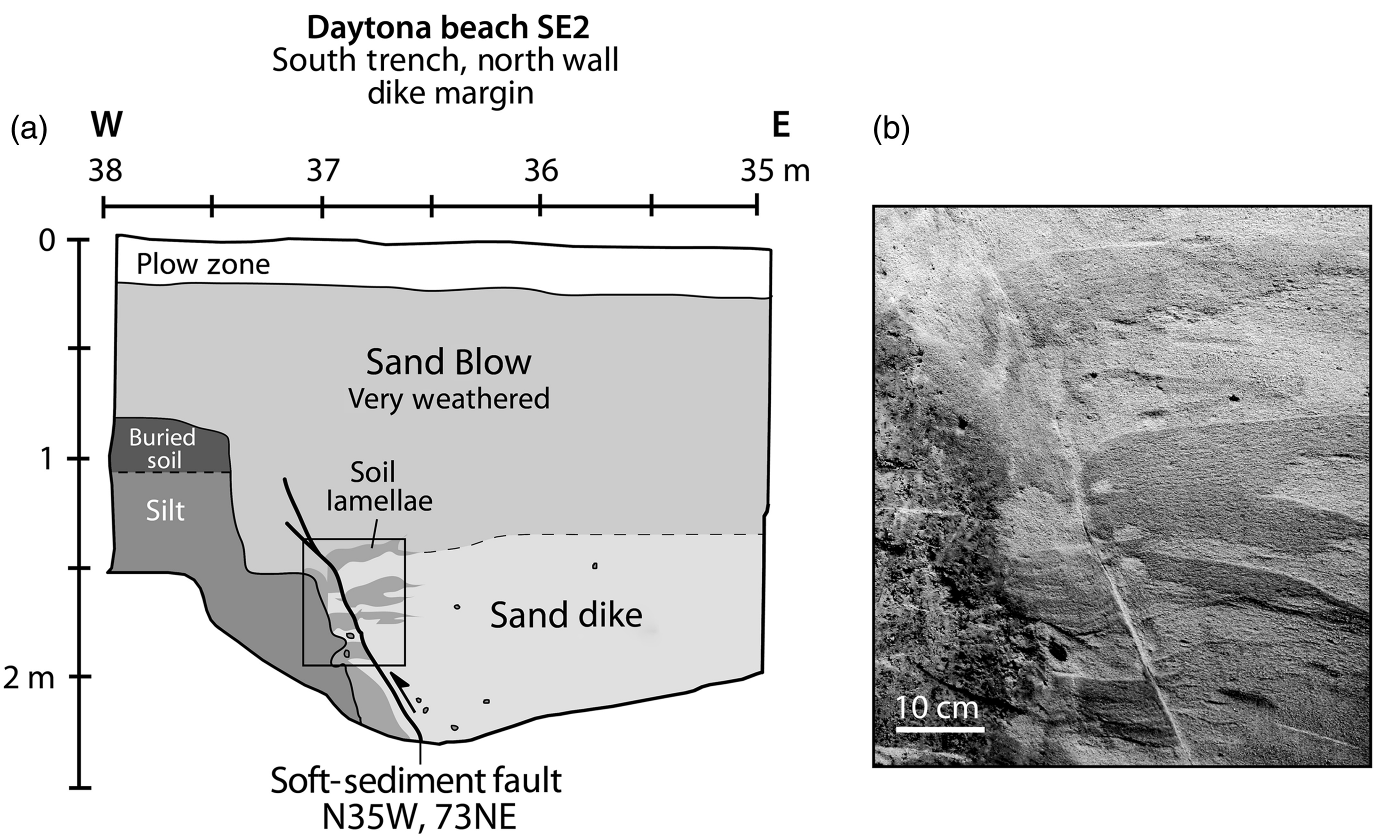

Figure 4. (a) Portion of trench log at site DBSE2 showing a weathered sand blow and the western margin of a sand dike below. Soil lamellae occur along the margin of the sand dike and appear to have been dragged along and offset by a soft-sediment fault (SSF). The fault has a strike and dip of N35°W, 73° NE, and parallels the DBL. (b) Photograph of the SSF along which soil lamellae are dragged and offset. The area of the photograph is outlined with a black rectangle on the adjacent log. Colored versions of the log and photograph are provided in Figure S5.

Liang and Forman, 2019). Results of OSL dating are presented in Tables S2–S5, the site investigation summaries, and trench logs in the supplemental material. Because of improvements in methodology (e.g., algorithms that optimize equivalent dose determinations and more robust statistical analyses to reduce errors) during the course of this study, OSL ages for samples collected at sites DBNW3 and DBNW5 were recalculated (Table S4). OSL ages reflect the statistical mean values with error ranges at 1 standard deviation.

To use both ^{14}C and OSL dating results to estimate the ages of liquefaction features and thus the timing of past earthquakes, ^{14}C ages with error ranges of 1 standard deviation are used in this analysis. Although both ^{14}C and OSL ages are considered in estimating the ages of the liquefaction features, ^{14}C ages are often given preference due to their stratigraphic positions and/or smaller error ranges. Age constraints and age estimates of sand blows, and thus the timing of events, are provided in Table 1 and in site investigation summaries in the supplemental material. ^{14}C and OSL ages are reported as before present (B.P.), meaning before A.D. 1950.

Evaluation of scenario earthquakes

Liquefaction potential analysis is performed for scenario earthquakes of various moment magnitudes (e.g., **M** 5.5, 6.0, 6.5, 7.0, and 7.5) to help assess the magnitudes of the Marianna paleoearthquakes that induced liquefaction in the Marianna area and at distal sites near Marked Tree and Blytheville, Arkansas, and Tunica, Mississippi (Figs. 1 and 2, Table 2). The distal sites of liquefaction were discovered during paleoliquefaction studies in the NMSZ and surrounding region (Tuttle, Wolf, *et al.*, 2019). They include small (10–25 cm thick) sand blows and related sand dikes at the Eaker 2 site north of Blytheville and at the Promised Land site northwest of Marked Tree that are similar in age (4.7 and 5.4 ka, respectively) to large sand blows in the Marianna area (Fig. 1). These liquefaction features are older and smaller than features attributed to New Madrid paleoearthquakes. In addition, three generations of small liquefaction features were found along the Coldwater River east of Tunica, Mississippi (Fig. 1). Two generations of the features overlap with the ages (4.7 and 6.8 ka) of large Marianna sand blows, and therefore, they may have formed as the result of Marianna paleoearthquakes (Tuttle, Wolf, *et al.*, 2019).

The cyclic stress method is used to assess liquefaction potential (e.g., Seed and Idriss, 1971; Juang and Jiang, 2000; Youd *et al.*, 2001; Cetin *et al.*, 2004; Robertson, 2010; Juang *et al.*, 2017), and regionally appropriate ground-motion prediction equations are used to calculate peak ground accelerations for scenario earthquakes (e.g., Atkinson and Boore, 2011; Atkinson and Assatourians, 2012). Geotechnical data used in the analysis were collected by the USGS, the Arkansas Department of Transportation, and the Mississippi Department of Transportation, and their borehole locations are shown in Figures 1 and 2. The geotechnical data were reviewed, and cohesionless sandy sediments between 5 and 20 m below the ground surface and with blow counts (a measure of soil density) of less than 30 were selected for analysis. The results of liquefaction potential analysis for scenario earthquakes are summarized in Table 2.

Results

Site investigations and dating of sand blows

Since 2006, paleoseismic investigations have been conducted at six sites of earthquake-induced liquefaction—DBSE2, DBNW2, DBNW3, DBNW5, DBNW7, and DBNW8—all along or close to the DBL and underlying fault zone (Fig. 2, Fig. S1). The investigations suggest that the fault zone produced large earthquakes about 4.7 ± 0.15 ka, 5.4 ± 0.1 ka, 9.8 ± 0.15 ka, <19.5 ka, and <24.3 ka (Table 1). DBSE2 and DBNW2 occur along the middle portion of the fault zone, and DBNW5, DBNW7, and DBNW8 are located toward the northern end of the fault zone. We have identified likely sand blows along the southern end of the fault zone, but have not been granted permission by property owners to excavate the sites. All the sand blows are very large, ranging from 36–100+m in width and from 60–300+m in length, with sand blows at DBSE2 and DBNW2 in the middle portion of the fault zone being especially large (Table 1).

Sand blows at all the study sites are obvious on satellite images and in the field. GPR surveys at the sites, image large sand blows, and sand dikes delineated by strong reflectors related to contacts between the liquefaction features and the silty soil (see Fig. 3). Trenches were excavated roughly perpendicular to the sand dikes as imaged by the GPR surveys. The trenches reveal sand blows ranging from 1 to 2.4 m thick and sand dikes ranging from 4 cm to 6.4 m wide. All the sand blows are weathered, some more than others (Table 1). Indicators of weathering include redoximorphic features (aka mottles) and related Fe–Mn nodules that form as a result of water-table fluctuations, rubification, or redding of the sand blows due to the release of iron and the formation of iron oxides that coat the sand grains, and soil lamellae, which result from the translocation and accumulation of silt usually along textural boundaries. Soils that would have developed in the sand blows over time are disturbed by plowing, and in some cases, removed by grading, which limits our ability to collect samples that would provide close minimum constraining ages for the sand blows. However, the sand blows bury soils that were at the ground surface at the time of the events; so, dating organic material such as twigs and leaves and residual carbon in the buried soils provides close and fairly close maximum constraining ages for the sand blows. The characteristics and age estimates of sand blows at the six sites are summarized below and in Table 1. More information about the site investigations, including satellite images, geophysical profiles, trench logs, and results of ^{14}C and OSL dating of samples collected at the sites, is provided in the supplemental material.

TABLE 2
Results of Evaluations of Marianna Scenario Earthquakes

Sites*	Map ID	Source-to-Site Distance (km)	Results†
1. Scenario earthquake M 5.5			
Borehole 1	BH1	5	N
Borehole 1	BH1	10	N
Borehole 2	BH2	5	N
Borehole 2	BH2	10	N
L'Anguille River	BH4	13	N
St. Francis River	BH5	37	N
2. Scenario earthquake M 6.0			
Borehole 1	BH1	5	L
Borehole 1	BH1	10	N
Borehole 2	BH2	5	L
Borehole 2	BH2	10	N
L'Anguille River	BH4	13	L
St. Francis River	BH5	37	N
3. Scenario earthquake M 6.5			
Borehole 1	BH1	5	L
Borehole 1	BH1	10	L
Borehole 2	BH2	5	L
Borehole 2	BH2	10	L
L'Anguille River	BH4	13	L
St. Francis River	BH5	37	L
Coldwater River (E. Tunica)	BH3	55	N
Ditch 10 (Promised Land)	BH6	105	N
4. Scenario earthquake M 7.0			
Coldwater River (E. Tunica)	BH3	55	L/N
Ditch 10 (Promised Land)	BH6	105	N
5. Scenario earthquake M 7.5			
Coldwater River (E. Tunica)	BH3	55	L
Ditch 10 (Promised Land)	BH6	105	L

*Liquefaction was observed in the vicinity of these sites.
†L indicates liquefaction likely for 45%–100% of the layers analyzed; L/N indicates marginal because liquefaction is predicted for 24%–44% of the layers analyzed; N indicates liquefaction not likely because liquefaction is predicted for less than 24% of the layers analyzed.

At site DBSE2, the sand blow is about 60 m wide, 140 m long, and 2.2 m thick and connected to at least seven sand dikes ranging in width from 7 cm to possibly as wide as 5 m (Fig. 3, Figs. S2–S4, Table 1). Weathering is especially pronounced in the upper 1 m of the sand blow, though the entire thickness of the sand blow is iron-stained and exhibits redoximorphic features with Fe–Mn nodules (Fig. 4, Fig. S5). Soil lamellae occur along the margins of sand dikes. In addition, fines have accumulated in the lower part of the sand blow above the buried soil and in several of the dikes. A soft-sediment fault (SSF) occurs adjacent to the western margin of a large sand dike and is subparallel to the DBL (Fig. 4, Figs. S4 and S5). Soil lamellae appear to have been dragged along and offset across the fault. Apparent vertical offset of soil lamellae and mismatch of lamellae thickness across the fault suggest reverse and strike-slip components of displacement. ^{14}C dating of charred material, C1, collected from the top of the soil buried by the large sand blow, yielded an age of 9680–9910 yr B.P. (Fig. S4, Tables S1). This represents a close maximum constraining age for the sand blow, indicating that it formed about 9.8 ka. Dating of sediment sample, OSL1, also collected from the buried soil and about 5 cm of the base of the sand blow, yielded an age of 11,940 ± 1,000 yr B.P., consistent with the slightly younger ^{14}C age for charred material collected higher in the buried soil (Fig. S4, Table S2).

At site DBNW2, the sand blow is exceptionally large, exceeding 100 m in width and 300 m in length (Fig. S6). Upon closer inspection, the sand blow is composed of two large sand blows of different ages that formed adjacent to each other along the DBL and underlying fault zone. The sand blow exposed in the south trench is 1.6 m thick and connected to a 6.4-m-wide dike (Figs. S7 and S8, Table 1). The sand blow is very weathered, especially the upper 0.5 m, and exhibits redoximorphic features and manganese staining. Silt has accumulated, and soil lamellae have formed along the eastern margin of the dike. The buried soil below the large sand blow is displaced downward about 1.5 m on the west side of the dike. Dating of sediment samples, OSL1 and OSL2, collected from the buried soil yielded ages of 15,040 ± 4,540 yr B.P. and 19,540 ± 1,010 yr B.P., respectively (Fig. S8, Table S3). The samples were collected from the same context, and their ages overlap at one sigma. However, the age of 19.54 ka for OSL2 has a smaller one sigma error (5%) than does the age of 15.04 ka for OSL1 (30%). Therefore, the age of 19.54 ka has greater significance and is preferred. The overdispersion value, or scatter of the equivalent dose value, is high (33%) for sample OSL2, suggesting that it may not have been completely reset before burial by the sand blow or may include older sediment mixed in from above or below. Therefore, the OSL age is interpreted as a maximum constraining age and suggests that the liquefaction event is younger than about 19.5 ka.

The sand blow exposed in the north trench at DBNW2 is 2.4 m thick and connected to a 4.5-m-wide dike (Fig. S9). The sand blow is extremely weathered, especially the upper 1 m, and exhibits redoximorphic features and iron staining. Silt has accumulated along the base of the sand blow above the buried soil, and a 1.5 m thick sequence of soil lamellae occurs along the eastern margin of the large dike. The buried soil below the sand blow is displaced downward about 1.2 m again on the west side of the dike. Two SSFs, adjacent and subparallel to the eastern margin of the sand dike, appear to offset the sequence of soil lamellae. Several domains of relatively unweathered, loose sand appear to have been injected along the faults. These observations suggest that a second event, including faulting and earthquake-induced liquefaction, occurred thousands of years after the first event responsible for the formation of the large sand blow and dike. The second event may be the same event responsible for the formation of the sand blow in the south trench. Dating of sediment samples, OSL1 and OSL2, collected from the soil buried by the sand blow returned ages of 32,440 ± 1,880 yr B.P. and 24,340 ± 1,790 yr B.P., respectively (Fig. S9, Table S3). Even though the samples were collected from the same context, the OSL ages differ by at least 4430 yr. Overdispersion values are modest (29%) for OSL1 and high (41%) for OSL2. The age for OSL1 may reflect the age of the parent material of the soil, whereas OSL2 may have been mixed sediment or poorly bleached. These ages are not well constrained but represent maximum limiting ages and suggest that the liquefaction event is younger than about 24.3 ka.

At site DBNW3, the sand blow, 52 m wide, 85 m long, and 1 m thick, is connected to at least two sand dikes (Figs. S10 and S11). The sand blow and the main sand dike are exposed in two trenches. The main dike is 17 cm wide in the north trench and up to 1 m wide in the south trench (Figs. S12 and S13). In both trenches, the soil buried by the sand blow is displaced downward on the east side of the dike by 10 cm in the north trench and by 40 cm in the south trench. Weathering is similar in both trenches, with iron staining in the upper 55–90 cm of the sand blow and the upper 15–25 cm of the main sand dike. A few Fe–Mn nodules and soil lamellae have formed in the upper 50 cm of sand blow. In the north trench, ^{14}C dating of charred material, C1, from the buried soil about 13 cm below the sand blow yielded an age of 4573–4805 yr B.P. (Fig. S12, Table S1). This represents a fairly close maximum constraining age of 4.7 ka for the sand blow. Dating of a sediment sample, OSL1, collected from the buried soil 3–5 cm below the sand blow yielded an age of 4710 ± 215 yr B.P. (Fig. S12, Table S4). This age is consistent with the ^{14}C age and supports the age estimate of 4.7 ka for the sand blow. Another sediment sample, OSL3, collected from the subsoil 33–38 cm below the sand blow yielded an OSL age of 13,310 ± 540 yr B.P., probably reflecting the age of the parent material. In the southern trench, a sediment sample, OSL1, collected from the subsoil 32–37 cm below the sand blow yielded an age of 12,500 ± 405 yr B.P., very similar to the age of the sediment sample collected from a similar context in the northern trench (Fig. S13, Table S4). All the sediment samples dated at this site have low overdispersion values (9%, 13%, and 9%), suggesting the sediment was not mixed and lending confidence in the age estimates.

At site DBNW5, the sand blow, 36 m wide, 64 m long, and 1.4 m thick, is connected to a large sand dike about 2.7 m wide (Figs. S14–S16). The sand blow and sand dike were exposed in two trenches, but torrential rain at the time of field work flooded the two trenches and caused them to collapse. The south trench was re-excavated to log the trench wall and to collect samples for dating. In the south trench, large clasts of clayey silt from the subsoil occur in the upper portion of the large sand dike, and the soil buried by the sand blow is displaced downward on the northeast side of the dike by about 1.1 m. Weathering in the sand blow includes iron staining and formation of small to medium Fe–Mn nodules in its upper 40 cm and large nodules above its basal contact with the buried soil. The formation of many small-to-large Fe–Mn nodules is probably related to water-table fluctuations at this relatively wet site. ^{14}C dating of organic-rich sediment samples, SL1 and SL2, from the top of the buried soil on both sides of the large dike provides fairly close maximum constraining ages of 5474–5577 yr B.P. and 5327–5476 yr B.P., respectively (Table S1). Giving preference to the younger ^{14}C age, the sand blow formed about 5.4 ka. Dating of a sediment sample, OSL3, collected from the top of the buried soil on the east side of the dike provides a close maximum constraining age of 5110 ± 120 yr B.P. (Table S5) and is in fairly close agreement with the ^{14}C ages of the organic samples collected in a similar context. A sediment sample, OSL4, collected 16 cm below the top of the buried soil, provides a maximum constraining age of 7475 ± 235 yr B.P. (Table S5). Sediment samples, OSL1 and OSL2, collected from the buried soil higher in the section on the west side of the dike have higher overdispersion values, suggesting that they are more likely to be mixed (Tables S4). Giving preference to the younger of the two ^{14}C ages, the sand blow at this site is estimated to have formed about 5.4 ka.

At site DBNW7, located ~2.4 km east of the DBL, the sand blow is about 45 m wide, 60 m long, and 1.5 m thick and connected to a 49 cm wide sand dike (Figs. S17–S19). A vent structure occurs above the sand dike and is filled with silty, very fine sand, which is finer grained than much of the sand blow and represents the final phase of venting. The sand blow is very weathered with redoximorphic features throughout and several areas of intense iron staining with small Fe–Mn nodules. The soil buried by the sand blow is displaced downward about 0.5 m on the east side of the dike. ^{14}C dating of charred material, C2, collected near the tip of a root cast that extended through the sand blow and into the buried soil below, provides a minimum constraining age for the sand blow of 1179 yr B.P. (Fig. S19, Table S1). Unfortunately, the upper 10 cm of the buried soil was very bioturbated, especially on the west side of the dike, making it difficult to sample an undisturbed portion of the buried soil for dating. Sediment sample, OSL2, collected from the upper 5 cm of the buried soil yielded an age of 41,445 ± 2,060 yr B.P. (Fig. S19,

TABLE 3
Magnitude Estimates for Marianna Paleoearthquakes

Earthquake	DBL*	St. Francis	Coldwater	Ditch 10	Blytheville†
4.7 ka	**M** 6.0–6.5		**M** 7.0–7.5		**M** ≥ 7.2
5.4 ka	**M** 6.0–6.5			**M** 7.5	
6.8 ka		**M** 6.0–6.5	**M** 7.0–7.5		
9.8 ka	**M** 6.0–6.5				
<19.5 ka	**M** 6.0–6.5				
<24.3 ka	**M** 6.0–6.5				

*These magnitude estimates are considered minimum values for earthquakes that could induce liquefaction along the Daytona Beach lineament (DBL). For each of the 9.8, <19.5, and <24.3 ka events, only one liquefaction site so far has been studied along the DBL; these magnitude estimates are also considered minimum values for these three events.
†From Tuttle *et al.* (2019b, 2020).

Table S5). Its overdispersion value (24% ± 3%) is modest, suggesting that the OSL age may reflect the age of the parent material of the soil, rather than the time of burial of the surface by this sand blow. Sediment sample, OSL3, collected 15 cm below the top of the buried soil, in which bioturbation was less severe, yielded an age of 7200 ± 180 yr B.P. Its uncertainty range was relatively small, and the overdispersion value was low (5% ± 1%), lending confidence in the age. The age of this sample is similar to that (7475 ± 235 yr B.P.) of the sample, OSL4, collected 16 cm below the top of the buried soil at site DBNW5 (Fig. S16). This suggests that the sand blow and dike at DBNW7 may have formed at the same time as the liquefaction features at DBNW5 or about 5.4 ka. Sediment samples, OSL1 and OSL4, were collected from the upper portion of the DBNW7 sand blow and yielded ages of 16,285 ± 1,395 yr B.P. and 17,205 ± 1,350 yr B.P., respectively (Fig. S19, Table S5). One of the samples, OSL4, had a low overdispersion value (4% ± 1%). Assuming the sand blow formed about 5.4 ka, the sediment of the upper part of the sand blow is much older. This suggests that luminescence of the sand was not reset during venting, and the sand blow reflects the age of the source layer. This could be due to the rapid deposition of the sand blow.

At site DBNW8, located ~0.5 km west of the DBL, the sand blow is about 65 m wide, 75 m long, and 1.05 m thick (Figs. S20–S22). The sand blow is connected to two sand dikes. The western dike is 54 cm wide, and the eastern compound dike is composed of two phases, 50 and 16 cm wide. Vent structures above the sand dikes are filled with very fine sandy silt, finer grained than much of the sand blow. Similar to DBNW7, the sand blow is very weathered with redoximorphic features common and several areas of intense iron staining. In addition, a few soil lamellae have developed in the sand blow. The soil buried by the sand blow is displaced downward about 0.3 m on the west side of the eastern dike. Dating of a sediment sample, OSL5, collected about 8 cm below the top of the buried soil, yielded an age of 6335 ± 150 yr B.P., which represents a maximum constraining age for the sand blow and related sand dikes (Fig. S22, Table S5). There is confidence in the age estimate of this sample, given its small uncertainty and low overdispersion value of 4% ± 1%. At nearby site DBNW5, sediment samples, OSL3 and OSL4, collected at the top of the buried soil and 16 cm below the sand blow yielded OSL ages of 5110 ± 120 yr B.P. and 7475 ± 235 yr B.P, respectively (Fig. S16). At site DBNW8, the sediment sample, OSL5, which yielded an age of 6335 ± 150 yr B.P. was collected 8 cm below the top of the buried soil, or at a depth halfway between the two samples at DBNW5. Therefore, it seems likely that the sand blow at DBNW8 formed during the same event or about 5.4 ka. Like the samples collected from the sand blow at DBNW7, sediment samples, OSL1 and OSL4, collected from the upper part of the sand blow at DBNW8 yielded ages much older (18,375 ± 495 yr B.P. and 18,605 ± 1,345 yr B.P., respectively) than the soil buried by the sand blow (Fig. S22, Table S5). Also these samples have high dispersion values of 40 ± 8 and 36 ± 6, respectively. Therefore, the sand that vented to the ground surface as a result of liquefaction may not have been solar reset, especially if deposited rapidly.

Liquefaction potential analysis

Considering Marianna scenario earthquakes, an **M** 5.5 earthquake located 5 km below liquefaction site DB1 is not likely to induce liquefaction even at the local geotechnical sites, boreholes 1 and 2 (Figs. 1 and 2, BH1 and BH2; Table 2); whereas an **M** 6.0 earthquake located at 5 km depth, is likely to induce liquefaction at BH1 and BH2 and at the L'Anguille River site, borehole 4 (BH4). An **M** 6.5 earthquake located at 10 km depth is likely to induce liquefaction at those same three sites and at the St. Francis River site, borehole 5 (BH5). An **M** 7.0 earthquake is likely to induce marginal liquefaction at the Coldwater River site east of Tunica, MS, borehole 3 (BH3), but not at the Ditch 10 site near Promised Land, AR, borehole 6 (BH6); whereas an **M** 7.5 earthquake is likely to induce liquefaction at both the Coldwater River and Ditch 10 sites (Table 2).

As discussed earlier, a Marianna paleoearthquake about 4.7 ka produced very large sand blows along the DBL, possibly sand dikes along the Coldwater River east of Tunica, and a small sand blow at Eaker 2 north of Blytheville (Fig. 1; Tuttle, Wolf, *et al.*, 2019; Tuttle, Al-Shukri, and Mahdi, 2020). If so, the 4.7 ka event may have been of **M** 7.0–7.5 according to liquefaction analysis (Table 3). A Marianna paleoearthquake about 5.4 ka produced very large sand blows along the DBL and possibly a small sand blow and related dikes at Promised Land northwest of Marked Tree, Arkansas. If so, this event may have been of **M** 7.5 according to the analysis. In addition, a Marianna paleoearthquake sequence about 6.8 ka produced a compound sand blow along the St. Francis Ditch north of Marianna and possibly a small sand blow and sand dikes along the Coldwater River in Mississippi. If so, the 6.8 ka event may have been of **M** 7.0–7.5 (Table 3). So far, liquefaction features produced by earlier events about 9.8 ka, <19.5 ka, and <24.3 ka have only been documented along the DBL. Therefore, initial magnitude estimates for these events are **M** 6.0–6.5. However, these magnitudes are considered minimum values because the sand blows are very large and likely also formed during very large earthquakes, **M** ≥ 7.

Discussion

Paleoliquefaction investigations

Previously, earthquakes about 4.7 and 5.5 ka were interpreted from large, weathered sand blows and related sand dikes at sites Nancy1, Nancy2, and DB1 west and southwest of the town of Marianna (Fig. 2). These sand blows and other large sand blows occur along a northwest-oriented tonal lineament interpreted as the surface expression of an active fault zone—here named the Daytona Beach fault zone (DBFZ)—and the likely source of the earthquakes responsible for many of the liquefaction features in the area (Al-Shukri *et al.*, 2005, 2006; Tuttle *et al.*, 2006). This interpretation was supported by the results of a subsequent seismic reflection study that identified a fault zone beneath the lineament (Odum *et al.*, 2016). An earthquake sequence about 6.8 ka was interpreted from a compound sand blow at site SF500 northeast of the town of Marianna. This liquefaction site occurs near the intersection of the EMRRFZ and WRFZ, which might have been the sources of the earthquakes.

The more recent investigation at site DBSE2 of a very large sand blow resulted in the identification of an additional paleoearthquakes about 9.8 ka (Table 1). The age estimate for this event is robust, given that it is based on both ^{14}C and OSL ages that are in close agreement. The investigation at site DBNW2 of two very large sand blows with different degrees of weathering, including soil rubification and formation of soil lamellae, suggests two earlier events about <19.5 and <24.3 ka, though their age estimates are not well constrained. The investigation at site DBNW3 corroborated the earlier finding of a paleoearthquake about 4.7 ka. The investigations at DBNW5, DBNW7, and DBNW8 led to a slight revision in the age estimate of the 5.5 ka event to 5.4 ka and a reduction in the uncertainty, or error range, of the event timing (Table 1). The two closely timed events, about 4.7 and 5.4 ka, are distinct. The age estimates for these events do not overlap at the two-sigma error range. In addition, the age estimates for both events are robust, given the close agreement of ^{14}C and OSL ages at sites DBNW3 and DBNW5.

Sites DBSE2, DBNW2, DBNW3, DBNW5, DBNW7, and DBNW8 all occur along the DBL (Fig. 2, Fig. S1). Many of the large sand dikes at these sites strike northwest-southeast, subparallel to the lineament. The DBL cuts across the topography, the Rondo and Dudley morphostratigraphic units, and Big Cypress Creek, and is subparallel to a major fault zone in the area, the WRFZ. As imaged in two seismic reflection lines, an active fault zone, the DBFZ, occurs directly below the DBL (Odum *et al.*, 2016). These relationships support the interpretation that the DBL and the large sand blows along the lineament are the surface expression of faulting of the DBFZ.

At DBSE2 and DBNW2, SSFs with northwest–southeast strikes crosscut large sand dikes and soil lamellae that developed in the dikes (Table 1). SSFs within liquefaction features would normally be attributed to ground failure related to liquefaction during or soon after the event. However, the faults at DBSE2 and DBNW2 clearly formed well after emplacement of the large dikes and sand blows. At DBNW2, a younger generation of sand dikes appears to have been injected along some of the faults during a subsequent event. Though liquefaction-related ground failure cannot be ruled out, an alternative interpretation is that the SSFs at DBSE2 and DBNW2 are fault tips that ruptured the surface, or close to it, during the subsequent events. This seems like a distinct possibility given the occurrence of the two sites along the DBL, the orientation of the SSFs subparallel to the lineament, and the presence of an active fault zone below the DBL (Fig. S1). The SSFs cannot be traced into the overlying sand blows, but this is not surprising given the degree of soil development in these features.

The alternative interpretation of the origin of the SSFs raises the question: could the large sand dikes in which the SSFs occur mark faults that ruptured to the surface during earlier events and were injected by a large volume of water and sand resulting from liquefaction, forming large sand dikes and sand blows that now mask the faults? This question could be tested by conducting additional geophysical surveys to better image the DBFZ in Quaternary deposits. If sites could be identified where the upward termination of faults was not masked by overlying sand blow deposits, the sites could be trenched to directly study the DBFZ and independently evaluate event timing.

On the basis of our current knowledge, the DBFZ repeatedly produced large earthquakes between 4.7 and 9.8 ka, during the Middle and Early Holocene, with recurrence times ranging from 700 to 4400 yr. The fault zone also may have produced two large earthquakes during the last 13,000 yr of the Late Pleistocene (0.0117–0.129 Ma; Cohen *et al.*, 2022). In addition, the EMRRFZ and WRFZ may have produced a sequence of earthquakes about 6.8 ka during the Middle Holocene. Therefore, the Marianna area, or Marianna seismic zone (MSZ), was active for 4000 yr, and possibly 20,000 yr, before entering an apparently

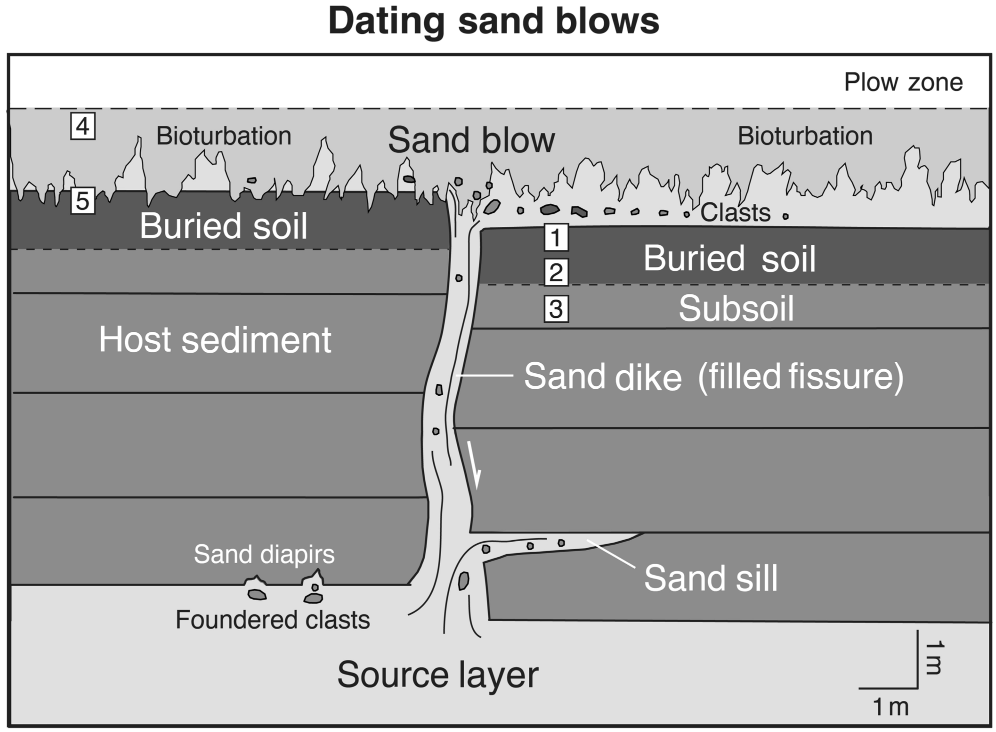

Sample	Description	Age constraint
1	Top of deeply buried soil and below zone of bioturbation: best place to collect 14C and OSL samples; 14C sample likely to be preserved; OSL sample likely to be exposed to sunlight prior to burial and less likely to be reworked	Close maximum
2	Within deeply buried soil and below zone of bioturbation: good place to collect 14C and OSL samples for same reasons given above, but would pre-date liquefaction	Maximum
3	From subsoil: 14C and OSL samples help to establish history of deposition of host sediment; also, provide maximum age constraint of liquefaction if no good samples collected from buried soil	Maximum
4	From sand blow: 14C sample of tree roots grown into sand blow would post-date liquefaction;	Minimum
	OSL sample not likely to be exposed to sufficient sunlight to reset luminesence; also, sediment bioturbated	Maximum; age of source layer
5	Top of less deeply buried soil and within zone of bioturbation: 14C sample less likely to be preserved; OSL sample likely to be reworked	Maximum

Figure 5. Diagram illustrating positions of samples for dating sand blows, descriptions of the effects of depth and bioturbation on the samples, and age constraint provided by the samples.

quiescent period about 4.5 ka. This timing coincides with the beginning of the active period in the NMSZ, suggesting that seismicity shifted from the MSZ to the NMSZ about 4.5 ka. If not, the MSZ may be overdue for a large earthquake.

The chronology of paleoearthquakes in the MSZ is likely to be complete for the Holocene, but incomplete for the Late Pleistocene. There are many more sand blows in the area that could be studied to better understand the Late Pleistocene earthquake history of the MSZ. However, identifying Late Pleistocene sand blows before trenching is challenging. Weathering characteristics of sand blows are useful indicators of age. We have found that the older sand blows and related dikes have deep weathering profiles, including development of rubification and soil lamellae, and accumulation of fines, especially above buried soils. Remote sensing may help differentiate sand blows by their degree of weathering. Currently, various remote sensing techniques are being tested in the MSZ.

A better understanding of the paleoearthquake history of the MSZ would improve our understanding of the recurrence times of large-magnitude earthquakes and the long-term behavior of the Marianna sources. In addition, the Marianna paleoearthquake history, combined with that of other areas, such as the NMSZ, would provide insights regarding the spatial and temporal migration of seismicity across the region. The NMSZ and the MSZ, both sources of repeated large-magnitude earthquakes, are characterized by the northeast-oriented Reelfoot Rift and northwest-oriented Proterozoic fault systems of which the WRFZ is a member, suggesting the two regions are structurally related. If so, their histories of stress buildup and release may be interrelated. Additional paleoliquefaction studies could provide longer-term earthquake chronologies that would test this relationship and improve seismic hazard assessments for the region.

Lessons learned about dating old sand blows

Important lessons have been learned about dating large, weathered sand blows. ^{14}C dating of plant material in the upper few centimeters of soil buried by a sand blow usually provides the best opportunity for establishing a close maximum constraining age for the sand blow, and thus, the causative earthquake (Fig. 5). However, plant material more than 5–10 ka is rarely preserved in buried soils in the Marianna area, especially in buried soils within 0.5–1.0 m of the ground surface. If no plant material can be found, thin (~0.25 cm) slices of the surface of the buried soil can be collected to date residual carbon in the soil. Residual carbon would have accumulated over a period of time, perhaps 10s–100s of years. Therefore, a soil sample can provide a fairly close maximum constraining age for a sand blow, but probably not as close an age as plant material buried immediately below the sand blow.

OSL dating of a buried soil can also provide fairly close maximum constraining ages for sand blows (Fig. 5). For OSL dating to provide a meaningful age estimate of the time of burial by the sand blow, however, the luminescence in the quartz grains has to be completely reset by exposure to the sun, like in buried A horizons. A potential problem is post-event bioturbation of the buried soil by roots, which can mix the soil both with vented sand above and subsoil below, and the OSL age would not reflect the time of burial. For the Marianna sand blows, bioturbation by roots often extends to 1.0–1.5 m below the ground surface. Therefore, samples collected below the zone of bioturbation are more likely to provide meaningful results.

Overdispersion, also known as scatter, is measured during the OSL dating process and often reflects the degree of solar resetting, mixing of grain populations, or variable dose rate environment with burial (Forman *et al.*, 2000; Galbraith and Roberts, 2012; Liang and Forman, 2019). For a sample collected from the A horizon of the buried soil, an OSL age with low overdispersion is more likely to reflect the time of burial by the sand blow. If overdispersion is >20%–25%, the minimum age model is used, which identifies the lowest equivalent dose population for >30 aliquots. This age may be a maximum limiting age. OSL ages of the sand blows are older than the time of their emplacement. Some of the OSL samples collected from the sand blows had high dispersion values, suggesting that they were mixed and/or partially solar reset. In these cases, we surmise that the rapid deposition of the sand blows prohibited complete solar resetting of the vented sand. Other samples yielded overdispersion values of <15%, indicating solar reset, and provided credible estimates of the pre-existing parent material of the soil.

The aeolian loess deposits that cap both Rondo and Dudley morphostratigraphic units were likely to have been solar reset at the time of deposition. Since then, soil formation would have progressed over time. Situated in a forested environment, only the uppermost few centimeters of the A horizons are likely to have been subjected to solar resetting. The Pleistocene terraces experienced little subsequent aeolian or fluvial deposition but were subjected to deformation caused by liquefaction-related ground failures and possibly faulting and to burial by sand blows. Therefore, sand blows are likely to have ages similar to the sandy fluvial deposits from which they were sourced, unless the vented sand was reset or partially reset during deposition.

Liquefaction-potential analysis or evaluation of scenario earthquakes

The sand blows and related sand dikes along the DBL are very large, similar in size to sand blows and dikes in the NMSZ, and their source sands are relatively deep (~12.5 m) (Al-Shukri *et al.*, 2015; Tuttle, Wolf, *et al.*, 2019). Therefore, it is likely that the earthquakes responsible for their formation are very large in the **M** 7.0–7.5 range. Very large earthquakes would be expected to induce liquefaction at considerable distances in sediment that tends to be susceptible to liquefaction, such as Holocene fluvial deposits. Therefore, it seems reasonable to interpret the small sand blows and sand dikes of similar age near Coldwater River, Promised Land, and Blytheville as distal liquefaction features resulting from very large Marianna earthquakes. There are geographical gaps, however, between the MSZ and the distal liquefaction sites, leading to uncertainty in this interpretation. A broader distribution of similar-age features would add confidence in the interpretation of the liquefaction fields and in magnitude estimates for the 4.7, 5.4, and 6.8 ka Marianna events. Therefore, additional reconnaissance for and study of paleoliquefaction features is recommended in the region surrounding the MSZ.

Conclusions

The main findings of this article are as follows:

- The Marianna chronology of paleoearthquakes is revised to about 4.7, 5.4, 6.8, 9.8 ka, and possibly two earlier events about <19.5 and <24.3 ka;
- the age estimates of the Middle-Early Holocene events are robust and have small error ranges of ±0.1–0.15 ka;
- the age estimates of the two possible Late Pleistocene events are not well constrained and require further study to improve confidence in the event timing;
- pre-event surface soils buried by sand blows that are more than 1.5 m thick offer the best opportunity to collect samples for ^{14}C and OSL dating that will provide close or fairly close maximum constraining ages for the sand blows and their causative earthquakes; and
- the DBFZ was the likely source of the about 4.7, 5.4, and 9.8 ka paleoearthquakes, and liquefaction potential analysis suggests that these events were of **M** 7.0–7.5.

Given the recent paleoseismic findings presented here, revisions may be warranted in the characterization of the Marianna earthquake source in the U.S. National Seismic Hazard Model. The revisions might include the addition of the DBFZ as a fault-zone source, reduction in uncertainty of the recurrence times for three Holocene earthquakes, addition of two possible Late

Pleistocene earthquakes, and a shift in magnitude toward very large earthquakes with heavier weighting of **M** 7.5.

Additional reconnaissance for and study of Holocene and Late Pleistocene sand blows in the Marianna area and the surrounding region will improve understanding of liquefaction fields and magnitudes of Marianna earthquakes, recurrence times of large-magnitude earthquakes, long-term behavior of the Marianna source, and spatial and temporal migration of seismicity along the Reelfoot Rift and across the central United States.

Data and Resources

Seismicity shown in Figures 1 and 2 is from the Center for Earthquake Research and Information available at https://folkworm.ceri.memphis.edu/catalogs/html/cat_nm.html. Also shown in Figures 1 and 2 are liquefaction features from this study and other studies conducted by Tuttle and collaborators. Geotechnical data were provided by Tom Holzer of the U.S. Geological Survey and the Arkansas and Mississippi Departments of Transportation. Otherwise, all data included in this article were collected by the authors or derived from other published sources listed in the references. Information about liquefaction sites, liquefaction features, and results of dating have been entered into databases that are available to the public for download as both Excel files and Shapefiles from https://mptuttle.com/databases.html. Both websites were last accessed in December 2025. The supplemental material for this article includes additional information related to the six study sites—DBSW2, DBNW2, DBNW3, DBNW5, DBNW7, and DBNW8—as follows: (1) a map showing ages and sizes of sand blows at the study sites along the Daytona Beach lineament and locations of two seismic-reflection profiles with interpreted fault zones projected to the surface, (2) site investigation summaries including satellite images, geophysical profiles, and trench logs for the sites, (3) tabulated results of radiocarbon (^{14}C) and optically stimulated luminescence dating for samples collected at the sites, and (4) a list of cited references. Satellite imagery used as site base maps is from Esri World Imagery and Google Earth, as noted in the figure captions.

Declaration of Competing Interests

The authors acknowledge that there are no conflicts of interest recorded.

Acknowledgments

The Office of the State Geologist of Arkansas facilitated and paid for the excavation of trenches. ^{14}C and optically stimulated luminescence dating were performed by Beta Analytic, Inc. and Geoluminescence Dating Research Lab at Baylor University or USGS OSL Lab, respectively. Thanks to the property owners and farmers who gave us permission to work at the study sites and to Ross Hartleb and Pilar Villamor for their thorough and thoughtful reviews that improved this article. Research presented in this article was supported by the National Earthquake Hazard Reduction Program managed by the USGS under Grants 1434–07HQGR0069, G12AP20093, G18AP00083, and G22AP00335. The views and conclusions contained in this document are those of the authors and should not be interpreted as representing the opinions or policies of the USGS.

References

Al-Qadhi, O. (2010). Geophysical investigation of paleoseismological features in eastern Arkansas, USA, *Ph.D. dissertation*, University of Arkansas at Little Rock, Little Rock, Arkansas, USA, 235 pp., plus Appendix A.

Al-Shukri, H., H. Mahdi, O. Al-Qadhi, and M. P. Tuttle (2009). Spatial and temporal characteristics of paleoseismic features in the southern terminus of the New Madrid seismic zone in eastern Arkansas, *Final Technical Rept. Prepared for U.S. Geol. Surv. Award 1434-07HQGR0069*, 24 pp.

Al-Shukri, H., H. Mahdi, and M. Tuttle (2006). Three-dimensional imaging of earthquake-induced features with ground penetrating radar, near Marianna, Arkansas, *Seismol. Res. Lett.* **77,** 505–513.

Al-Shukri, H., H. Mahdi, M. P. Tuttle, and K. Dyer-Williams (2015). Geophysical and paleoseismic investigations of large sand blows along a northwest-oriented lineament near Marianna, Arkansas, *Final Technical Rept. Prepared for U.S. Geol. Surv. Award G12AP20093*, 31 pp.

Al-Shukri, H. J., R. E. Lemmer, H. H. Mahdi, and J. B. Connelly (2005). Spatial and temporal characteristics of paleoseismic features in the southern terminus of the New Madrid seismic zone in eastern Arkansas, *Seismol. Res. Lett.* **76,** 502–511.

Atkinson, G., and K. Assatourians (2012). GMPEs for national hazard maps (Miscellaneous resources), available at https://www.seismotoolbox.ca/index.html (last accessed December 2025).

Atkinson, G., and D. Boore (2011). Modification to existing ground-motion prediction equations in light of new data, *Bull. Seismol. Soc. Am.* **101**, 1121–1135.

Bronk Ramsey, C. (2009). Bayesian analysis of radiocarbon dates, *Radiocarbon* **51,** 337–360.

Cetin, K. O., R. B. Seed, A. K. Der Kiureghian, K. Tokimatsu, L. F. Harder Jr., R. E. Kayen, and R. E. S. Moss (2004). SPT-based probabilistic and deterministic assessment of seismic soil liquefaction potential, *J. Geotech. Geoenviron. Eng.* **130,** 1314–1340.

Chlaib, H. K., H. Mahdi, H. J. Al-Shukri, M. Su, A. Catakli, and N. Abd (2014). Using ground penetrating radar to detect small-scale animal burrows, *J. Appl. Geophys.* doi: 10.1016/j.jappgeo.2014.01.011.

Cohen, K. M., S. C. Finney, P. L. Gibbard, and J.-X. Fan (2022). The ICS international chronostratigraphic chart, *Episodes* **36,** 199–204.

Forman, S. L., J. Pierson, and K. Lepper (2000). Luminescence geochronology, *Quat. Geochronol.* **4,** 157–175.

Galbraith, R. F., and R. G. Roberts (2012). Statistical aspects of equivalent dose and error calculation and display in OSL dating: An overview and some recommendations, *Quat. Geochronol.* **11,** 1–27.

Gray, J. L. (1977). Soil survey of Lee County, Arkansas, U.S. Department of Agriculture, Soil Conservation Service and Forest Service, in Cooperation with the Arkansas Agricultural Experiment Station, 94 pp., plus 50 map sheets.

Hildenbrand, T. G., and J. D. Hendricks (1995). Geophysical setting of the Reelfoot Rift and relations between rift structures and the New Madrid seismic zone, *U.S. Geol. Surv. Profess. Pap. 1538-E*.

Hough, S. E. (2004). Scientific overview and historical context of the 1811-1812 New Madrid earthquake sequence, *Ann. Geophys.* **47,** 523–537.

Juang, C. H., and T. Jiang (2000). Assessing probabilistic methods for liquefaction potential evaluation, *Proc. of GeoDenver Conference,* *"Soil Dynamics and Liquefaction 2000"*, American Society of Civil Engineers, Reston, Virginia.

Juang, C. H., J. Zhang, S. Khoshnevisan, and W. Gong (2017). Probabilistic methods for assessing soil liquefaction and effect, *Geo-Risk 2017: Keynote Lectures*, American Society of Civil Engineers, 122–145, doi: 10.1061/9780784480694.

Liang, P., and S. L. Forman (2019). LDAC: An excel-based program for luminescence equivalent dose and burial age calculations, *Ancient TL* **37,** 21–40.

McKay, E. D., III (1979). Wisconsin loess stratigraphy of Illinois, in *Wisconsinan, Sangamonian, and Illinoian stratigraphy in Central Illinois*, L. R. Follmer, E. D. McKay, J. A. Lineback, and J. A. D. L. Gross (Editors), Illinois State Geological Survey, Champaign, IL, Guidebook, Vol. 13, 95–108.

Obermeier, S. F. (1989). The New Madrid earthquakes: an engineering-geologic interpretation of relict liquefaction features, *U.S. Geol. Surv. Profess. Pap. 1336-B*.

Odum, J. K., R. A. Williams, W. J. Stephenson, M. P. Tuttle, and H. Al-Shukri (2016). Preliminary assessment of a previously unknown fault zone beneath the Daytona Beach sand blow cluster near Marianna, Arkansas, *Seismol. Res. Lett.* **87,** 1453–1464.

Petersen, M. D., A. D. Frankel, S. C. Harmsen, C. S. Mueller, K. M. Haller, R. L. Wheeler, R. L. Wesson, Y. Zeng, O. S. Boyd, D. M. Perkins, *et al.* (2014). Documentation for the 2014 Update of the United States National Seismic Hazard Maps, *U.S. Geol. Surv. Open-File Rept. 2014–1091*, 243 pp.

Rains, D. S., and M. J. Guccione (2016). Formation of the Marianna Gap, a transverse stream valley, through Crowley's Ridge, northern Mississippi alluvial valley, U.S.A., *Seismol. Res. Lett.* **87,** 1442–1452.

Reimer, P. J., W. E. N. Austin, E. Bard, A. Bayliss, P. G. Blackwell, C. Bronk Ramsey, M. Butzin, H. Cheng, R. L. Edwards, M. Frederick, *et al.* (2020). The IntCal20 northern hemisphere radiocarbon age calibration curve (0-55 cal kBP), *Radiocarbon* **62,** 725–757. doi: 10.1017/RDC.2020.41.

Rittenour, T. M., M. D. Blum, and R. J. Goble (2007). Fluvial evolution of the lower Mississippi River valley during the last 100 k.y. glacial cycle: Response to glaciation and sea-level change, *GSA Bull.* **119,** 586–608, doi: 10.1130/B25934.1.

Robertson, P. K. (2010). Evaluation of flow liquefaction and liquefied strength using the CPT, *J. Geotech. Geoenviron. Eng.* **136,** 842–853.

Ruhe, R. V. (1983). Depositional environment of late Wisconsin loess in the midcontinental United States, in *Late-Quaternary Environments of the United States, 1, The Pleistocene*, S. C. Porter (Editor), University of Minnesota Press, Minneapolis, Minnesota, 130–137.

Saucier, R. T. (1977). Effects of the New Madrid earthquake series in the Mississippi alluvial valley, *U.S. Army Corps of Engineers Waterways Experiment Station Misc. Pap. S-77-5*, 10 pp.

Schumm, S. A., and W. J. Spitz (1996). Geological influences on the lower Mississippi River and its alluvial valley, *Eng. Geol.* **45,** 245–261.

Seed, H. B., and I. M. Idriss (1971). Simplified procedure for evaluating soil liquefaction potential, *J. Geotech. Eng. Div.* **97,** 1249–1273.

Technical Report (2012). Central and Eastern United States seismic source characterization for nuclear facilities, EPRI, U.S. DOE, and U.S. NRC, Palo Alto, California.

Thompson Jobe, J., A. Hatem, R. Gold, C. DuRoss, N. Reitman, R. Briggs, and C. Collett (2022). Revised earthquake geology inputs for the central and eastern United States and southeast Canada for the 2023 National Seismic Hazard Model, *Seismol. Res. Lett.* **93,** 3100–3120, doi: 10.1785/0220220162.

Thompson Jobe, J., A. Hatem, R. Gold, C. DuRoss, N. Reitman, R. Briggs, and C. Collett (2022). Revised earthquake geology inputs for the central and eastern United States and southeast Canada for the 2023 U.S. 50-State National Seismic Hazard Model, *Seismol. Res. Lett.* **93,** 3100–3120, doi: 10.1785/0220220162.

Tuttle, M. P., and R. Hartleb (2012). Appendix E. Central and Eastern U.S. paleoliquefaction database, uncertainties associated with paleoliquefaction data, and guidance for seismic source characterization, *The Central and Eastern U.S. Seismic Source Characterization for Nuclear Facilities*, EPRI, U.S. DOE, and U.S. NRC, Palo Alto, California, 135 pp. plus database.

Tuttle, M. P., H. Al-Shukri, and H. Mahdi (2006). Very large earthquakes centered southwest of the New Madrid seismic zone 5,000-7,000 years ago, *Seismol. Res. Lett.* **77**, 664–678.

Tuttle, M. P., H. Al-Shukri, and H. Mahdi (2020). Geophysical and paleoseismic investigations of large sand blows along a northwest-oriented lineament near Marianna, Arkansas, *Final Technical Rept. U.S. Geol. Surv. award G18AP00083*, 31 pp.

Tuttle, M. P., R. Hartleb, L. Wolf, and P. W. Mayne (2019). Paleoliquefaction studies and the evaluation of seismic hazard, *Geosciences* **9,** 61, doi: 10.3390/geosciences9070311.

Tuttle, M. P., L. W. Wolf, K. Dyer-Williams, P. W. Mayne, R. H. Lafferty, K. Hess, M. E. Starr, M. Haynes, J. Morrow, *et al.* (2019). Paleoliquefaction studies in moderate seismicity regions with a history of large earthquakes, *U.S. Nuclear Regulatory Agency, NUREG/CR-7257*, 450 pp.

Van Arsdale, R., and W. Cupples (2013). Late Pliocene and quaternary deformation of the reelfoot rift, *Geosphere* **9**, 1819–1831.

Wheeler, R. L., E. M. Omdahl, R. L. Dart, G. D. Wilkerson, and R. H. Bradford (2003). Earthquakes in the central U.S., 1699–2002, *U. S. Geol. Surv. Geol. Investig. Ser. I-2812*.

Youd, T. L., I. M. Idriss, R. D. Andrus, I. Arango, G. Castro, J. T. Christian, R. Dobry, W. D. L. Finn, L. F. Harder, Jr., and M. E. Hynes, *et al.* (2003). Liquefaction resistance of soils: Summary report from the 1996 NCEER and 1998 NCEER/NSF workshops on evaluation of liquefaction resistence of soils, *J. Geotech. Geoenviron. Eng.* **127,** 817–833.

Manuscript received 19 September 2025
Published online 14 January 2026